NASA Technical Memorandum 81471

SPECTRAL STRUCTURE OF PRESSURE MEASUREMENTS MADE IN A COMBUSTION DUCT

J. H. Miles
Lewis Research Center
Cleveland, Ohio

and

D. D. Raftopoulos
University of Toledo
Toledo, Ohio

Prepared for the
Ninety-ninth Meeting of the Acoustical Society of America
Atlanta, Georgia, April 21-25, 1980

SPECTRAL STRUCTURE OF PRESSURE MEASUREMENTS MADE IN A COMBUSTION DUCT

by

J. H. Miles
National Aeronautics and Space Administration
Lewis Research Center
Cleveland, Ohio

and

D. D. Raftopoulos
University of Toledo
Toledo, Ohio

ABSTRACT

The spectral structure of pressure measurements made in a ducted combustion test facility are studied. Dispersion and attenuation of acoustic plane waves may occur in the duct at low frequencies due to combustor emissions and affect the spectral structure. A model that considers the propagation of plane waves through a cloud of particles in a flowing gas and which includes heat transfer between soot particles and the gas is discussed. Experimental results are compared with theory.

NOMENCLATURE

A,B,C,D	matrices
a,b	velocity potential wave equation integration coefficients
$a_{m,n}$	pressure and velocity wave equation coefficients
$\mathscr{B}$	boundary condition operator
C_o	source spectrum coefficient
c	sound propagation velocity, m/sec
c_o	isentropic speed of sound, m/sec
c_p	gas specific heat at constant pressure, J/kg-K
d	diameter, m

E	acoustic energy density, J/m^3
f	frequency, Hz
$\mathcal{G}(\omega,w,y)$	solution in source region
$G(\omega,x)$	source term
$\mathcal{H}(\omega)$	source term coefficient
H	heat transfer coefficient, W/m^2-K
i	$(-1)^{\frac{1}{2}}$
$\mathcal{J}$	energy per unit mass, J/kg
k	propagation wave number, w/c, m^{-1}
$L,\mathcal{L}$	second order space differential equation operator
L_c	combustor length
M	Mach number, u/c
m_s	soot particle mass, kg
Nu_H	heat transfer Nusselt number, Hd/k
N	acoustic energy flux
n	number of particles per unit volume
PL	pressure level, dB
p	pressure, N/m^2
$\dot{Q}$	heat transferred to gas from particles by convection
$Q(-i\omega,ik,\Omega)$	time and space Fourier transform of q
$\vec{q}$	system state vector
$\mathcal{R}$	gas constant, J/kgn K
R	reflection factor
r	radius, m
$\mathcal{S}(\omega)/c_p$	transfer function for response of entropy source to a pressure perturbation
S	area, m^2

s	entropy of gas, J/kg-K
t	temperature, K
u	velocity of bulk gas, m/sec
$\bar{W}$	Wronskian
w	mass flux, kg/m^2 sec
x	cartesian coordinate, m
$\vec{Y}$	acoustic state vector
Z	acoustic impedance, mks Rayles
α	acoustic attenuation coefficient, dB/m
$\alpha_{m,n}$	duct transfer matrix element
$\beta_{m,n}$	discontinuity transfer matrix element
γ	specific heat ratio of gas
Δ	time and space Fourier transform of D/Dθ
ε	see Eq. (64)
ζ	see Eq. (65)
$\eta_{j\ell}$	see Eq. (30)
θ	time, sec
κ	gas thermal conductivity, W/m-K
κ_s	soot particle mass fraction, nm/ρ_o
ν	$2kr_d/\sqrt{1 - M^2}$
ρ	gas density, kg/m^3
τ_s	soot particle thermal relaxation time, $\dfrac{m_s c_p}{4\pi r_s^2 \left(\dfrac{Nu_H}{d_s}\right) \kappa}$
$\Phi[\ ]$	Fourier time transform operator
ϕ	reflection factor phase angle, degrees
ψ	velocity potential function
Ω	velocity potential wave number factor
ω	angular frequency, radians/sec

Superscripts and subscripts:

$\dot{(\ )}$	time average
$\vec{(\ )}$	vector quantity
$\overline{(\ )}$	instantaneous quantity
$(\ )^{+}$	upstream propagating
$(\ )^{-}$	downstream propagating
$(\ )^{o}$	wave propagating with flow
$(\ )_{CE}$	combustor exit
$(\ )_{CI}$	combustor inlet
$(\ )_{d}$	exit of duct system
$(\ )_{i}, (\ )_{j}$	identifies an axial duct location
$(\ )_{\ell}$	identifies source location
$(\ )_{m,n}$	elements of a matrix
$(\ )_{s}$	property of or due to soot particle
$(\ )_{o}$	reference state quantity
$(\ )_{1}$	perturbed quantity
$(\ )_{\infty}$	property far from soot particle

INTRODUCTION

As part of a combustion noise research program, pressure measurements were made in a liquid fuel ducted combustion test facility at the NASA Lewis Research Center. A schematic of the test facility is shown in Fig. 1. An analysis of the effect of the ducting downstream of the combustor on the measured pressure spectra using the adiabatic speed of sound showed the peaks in the measured spectra did not occur at frequencies corresponding to the predicted resonant frequencies. This paper first develops an acoustic wave equation that takes into account the presence of oxidizing soot particles which cause attenuation and a decrease in the sound propagation speed. Then

this acoustic wave equation and the duct geometry are used to model sound propagation in the ducted combustion system.

The literature contains a number of theoretical and experimental studies of the propagation of a plane wave through a cloud of particles in a stationary gas for various types of particles. Studies considering viscous and thermal interaction but not mass transfer were made by Epstein and Carhart (Ref. 1), Chow (Ref. 2), Temkin and Dobbins (Ref. 3), Dobbins and Temkin (Ref. 4), and Morfey (Ref. 5). Studies that consider vapor mass transfer in addition to viscous and thermal interaction were made by Cole and Dobbins (Ref. 6), Marble and Wooten (Ref. 7), Davidson (Ref. 8), and Marble and Candel (Ref. 9). Miles and Raftopoulos (Ref. 10) considered mass transfer due to soot oxidation in addition to viscous and thermal interaction. The theory of Cole and Dobbins (Ref. 6) was confirmed experimentally by Cole and Dobbins (Ref. 11). These studies have the objective of investigating attenuation and dispersion in a stationary, infinite bulk gas containing particles. In contrast, this paper studies the effect of attenuation and dispersion on duct spectra measurements in a flowing, confined gas containing soot particles.

Miles and Raftopoulos (Ref. 10) using Stokes' viscous drag law showing the effect of viscous interaction between the soot particles and bulk gas is not important at combustion noise frequencies. They also estimate the sound propagation speed from pressure cross spectra phase angle measurements. The estimated sound propagation speed is near the isothermal sound propagation speed, which indicates that heat transfer between the soot particles and the bulk gas may be more important than mass transfer at combustion noise frequencies. Consequently, the model presented herein includes only the heat transfer between soot particles and the flowing gas.

In the first part of this paper, the model is presented. This problem is first formulated as a distributed system parameter identification problem

with a single unknown parameter. An extensive review of the distributed system parameter identification problem is given in Ref. 12. Rather than using any of the methods described in Ref. 12, it is shown that for the problem discussed herein the solution can be approximated by the solution to an acoustic wave equation. This acoustic wave equation and its solution are used to model the duct system. Next, experimental results are presented. Last, the experimental and theoretical results are compared.

ANALYTICAL MODEL

Governing Equations

The following assumptions are used in this analysis:

(1) Fluctuations in the gas of pressure, velocity, density, entropy, and temperature are assumed to be small compared with their equilibrium values so that their squares and cross products may be neglected.

(2) The bulk gas is a perfect gas.

(3) The soot particles are sperical, non-porous, and of a uniform temperature and size.

(4) The volumetric heat transfer rate in a volume element containing a large number of soot particles is the sum of the effects due to each particle.

(5) Mass transfer and the body force due to viscous drag can be neglected. In addition the consequences of soot particle surface oxidation are idealized as producing a constant time-independent soot particle temperature.

The one-dimensional continuity, momentum, and energy equations for the bulk gas are as follows:

$$\frac{\partial \overline{\rho}}{\partial \theta} + \frac{\partial}{\partial x}\left(\overline{\rho}\ \overline{u}\right) = 0 \tag{1}$$

$$\overline{\rho}\ \frac{D\overline{u}}{D\theta} = -\frac{\partial \overline{p}}{\partial x} \tag{2}$$

$$\bar{p}\,\bar{t}\,\frac{D\bar{s}}{D\theta} = n\,\dot{\bar{Q}} \tag{3}$$

where the heat transfer rate per soot particle from the particle into a unit volume of gas is

$$\dot{\bar{Q}} = \left(4\pi r_s^2\right)\left(\frac{Nu_H}{d_s}\right)\kappa\,\left(\bar{t}_s - \bar{t}_\infty\right) \tag{4}$$

and the total derivative is given by

$$\frac{D}{D\theta} = \frac{\partial}{\partial\theta} + u_o\,\frac{\partial}{\partial x} \tag{5}$$

where the first term on the right hand side is the temporal member and the second term is the convective member in the x direction. When the entropy is constant the convective term is neglected if the time to convect a disturbance through the volume of interest is large compared with the time required for a quantity to change from a minimum to a maximum. The entropy is not constant in this problem since heat transfer between the soot particles and gas is taken into account. Therefore the effect on the spectrum of the convective term and heat transfer term may be of the same order of magnitude. Consequently, the convective term is included in the governing equations.

The gas equation is

$$\bar{p} = \bar{\rho}\,\mathscr{R}\,\bar{t} \tag{6}$$

and the adiabatic speed of sound is

$$c_o^2 = \gamma\,\mathscr{R}\,t_o = \gamma\,\frac{p_o}{\rho_o} \tag{7}$$

Equations (1) to (4) are linearized by considering small perturbations of the variables from their equilibrium values as follows:

$$\bar{p} = p_o + p_1 \tag{8}$$

$$\bar{u} = u_o + u_1 \tag{9}$$

$$\bar{p} = p_o + p_1 \tag{10}$$

$$\bar{t}_\infty = t_{o,\infty} + t_{1,\infty} \tag{11}$$

$$\bar{t}_s = t_{o,s} \tag{12}$$

$$\bar{s} = s_o + s_1 \tag{13}$$

Substitution of the above equations into Eqs. (1) to (4) and elimination of squares and cross products yields a set of linearized equations which can be written in the following non-dimensional form:

$$\frac{D}{D\theta}\left(\frac{\rho_1}{\rho_o}\right) + c \frac{\partial}{\partial x}\left(\frac{u_1}{c_o}\right) = 0 \tag{14}$$

$$\frac{D}{D\theta}\left(\frac{u_1}{c_o}\right) = -c_o \frac{\partial}{\partial x}\left(\frac{p_1}{\gamma p_o}\right) \tag{15}$$

$$\frac{D}{D\theta}\left(\frac{s_1}{c_p}\right) = -\frac{\kappa_s}{\tau_s}\frac{t_{1,\infty}}{t_{o,\infty}} \tag{16}$$

Where the particle mass fraction, κ_s, is a non-dimensional group of parameters defined as

$$\kappa_s = n m_s / \rho_o \tag{17}$$

and the heat transfer time constant is defined as

$$\tau_s = \frac{m_s c_p}{\left(4\pi r_s^2\right)\left(Nu_H/d_s\right)\kappa} \tag{18}$$

The system model thus depends on the ratio of two parameters. Herein, it is assumed that the heat transfer time constant parameter is a known parameter. Consequently, the particle mass fraction remains the single parameter to be identified.

These equations are simplified further using small perturbation thermodynamic relations. The ideal gas entropy equation is for small perturbations

$$\frac{s_1}{c_p} = \frac{1}{\gamma}\frac{p_1}{p_o} - \frac{\rho_1}{\rho_o} \tag{19}$$

Also, for small perturbations the gas equation of state is

$$\frac{p_1}{p_o} = \frac{\rho_1}{\rho_o} + \frac{t_{1,\infty}}{t_{o,\infty}} \tag{20}$$

Equations (19) and (20) are substituted into Eq. (16) to determine the response of the gas temperature to a pressure perturbation. Thus

$$\frac{D}{D\theta}\left(\frac{s_1}{c_p}\right) = \frac{D}{D\theta}\left(\frac{p_1}{\gamma p_o} - \frac{\rho_1}{\rho_o}\right) = \frac{D}{D\theta}\left[\frac{(1-\gamma)}{\gamma p_o}\, p_1 + \frac{t_{1,\infty}}{t_{o,\infty}}\right] = -\frac{\kappa_s t_{1,\infty}}{\tau_s t_{o,\infty}} \tag{21}$$

From Eq. (21) the desired relation is

$$\left(\frac{D}{D\theta} + \frac{\kappa_s}{\tau_s}\right)\frac{t_{1,\infty}}{t_{o,\infty}} = -\frac{D}{D\theta}\left(\frac{1-\gamma}{\gamma}\right)\frac{p_1}{p_o} \tag{22}$$

To remove the density perturbation, Eq. (19) is substituted into Eq. (14). Thus

$$\frac{D}{D\theta}\left(\frac{1}{\gamma}\frac{p_1}{p_o} - \frac{s_1}{c_p}\right) + c_o\frac{\partial}{\partial x}\left(\frac{u_1}{c_o}\right) = 0 \tag{23}$$

Solving Eq. (23) for s_1/c_p yields

$$\frac{D}{D\theta}\left(\frac{1}{\gamma}\frac{p_1}{p_o}\right) - c_o \frac{\partial}{\partial}\left(\frac{u_1}{c_o}\right) = \frac{D}{D\theta}\left(\frac{s_1}{c_p}\right) \tag{24}$$

State Variable Formulation

The system differential equation based on the small perturbation approximation is discussed next. Equations (15), (16), (22), and (24) are written in state variable form as

$$A \frac{\partial}{\partial \theta} \vec{q} + Bu_o \frac{\partial}{\partial x} \vec{q} + C\vec{q} = 0 \tag{25}$$

where

$$A = \begin{bmatrix} 1-\gamma & 0 & 0 & 1 \\ 0 & 1 & 0 & 0 \\ 0 & 0 & 1 & 0 \\ 1 & 0 & -1 & 0 \end{bmatrix} \tag{26}$$

$$B = \begin{bmatrix} 1-\gamma & 0 & 0 & 1 \\ c_o/u_o & 1 & 0 & 0 \\ 0 & 0 & 1 & 0 \\ 1 & c_o/u_o & -1 & 0 \end{bmatrix} \tag{27}$$

$$C = \begin{bmatrix} 0 & 0 & 0 & \kappa_s/\tau_s \\ 0 & 0 & 0 & 0 \\ 0 & 0 & 0 & \kappa_s/\tau_s \\ 0 & 0 & 0 & 0 \end{bmatrix} \tag{28}$$

$$\vec{q} = \begin{bmatrix} p_1/\gamma p_o \\ u_1/c_o \\ s_1/c_p \\ t_{1,\infty}/t_{o,\infty} \end{bmatrix} \tag{29}$$

The state variable solution to Eq. (25) is assumed to have the form

$$q_j(x,\theta) = \sum_{\ell=1}^{4} \eta_{j\ell} e^{(ik_o\Omega)_\ell x - i\omega\theta} \tag{30}$$

Taking the Fourier transform in the time variable and the space variable of Eq. (25) produces a set of four homogeneous algebraic equations in four unknowns expressed by the following matrix equation

$$[\bar{A}(-i\omega) + B(ik_o\Omega)u_o + \bar{C}]Q(-i\omega, ik_o\Omega) = 0 \tag{31}$$

A non-trivial solution to Eq. (31) exists if and only if the following determinant of the coefficient matrix vanishes:

$$\begin{bmatrix} \Delta(1-\gamma) & 0 & 0 & \Delta + \frac{\kappa_s}{\tau_s} \\ (ik_o\Omega)c_o & \Delta & 0 & 0 \\ 0 & 0 & \Delta & \kappa_s/\tau_s \\ \Delta & c_o(ik_o\Omega) & -\Delta & 0 \end{bmatrix} = 0 \tag{32}$$

where

$$\Delta = (-i\omega) + (ik_o\Omega)u_o \tag{33}$$

Solving the determinant equation yields a third order polynomial wave number equation for $(ik_o\Omega)$,

$$\left(\frac{\Lambda}{c_o}\right)^2 \left[1 - \frac{(1-\gamma)}{\left(\frac{\tau_s}{\kappa_s}\Lambda + 1\right)}\right] = (ik_o\Omega)^2 \tag{34}$$

and a solution $\Lambda = 0$ which corresponds to a wave number

$$(ik_o\Omega)_a^o = i\,\frac{\omega}{u_o} \tag{35a}$$

The roots of the third order polynomial can be found numerically to great accuracy using an iteration method due to Muller (Ref. 13). For the data studies herein the Mach number is low and a good approximate solution at all frequencies is

$$(ik_o\Omega)_b^o = -\frac{\kappa_s}{\tau_s} + i\,\frac{\omega}{u_o} \tag{35b}$$

$$(ik_o\Omega)^+ = \frac{i(\omega/c_s)}{M_s + 1} \tag{36}$$

$$(ik_o\Omega)^- = -\,i\,\frac{(\omega/c_s)}{1 - M_s} \tag{37}$$

where

$$c_s = \frac{c_o}{\left[1 + \frac{(\gamma-1)}{\left(1 - \frac{\tau_s}{\kappa_s} i\omega\right)}\right]^{1/2}} \tag{38}$$

and

$$M_s = \frac{u_o}{c_s} \tag{39}$$

By definition, the propagation velocity is related to the wave number equation by

$$c(\omega) = \frac{\omega}{\mathrm{Im}(ik_o\Omega)},\ \mathrm{m/sec} \tag{40}$$

Also by definition, the acoustic energy attenuation coefficient in Nepers per meter is

$$\alpha = -2\mathrm{Re}(ik_o\Omega) \tag{41}$$

Nepers per meter is converted to decibels per meter by multiplying by 10 log e = 4.34:

$$\alpha = -8.68\ \mathrm{Re}(ik_o\Omega) \tag{42}$$

The state variable solution to Eq. (25) is expressed in terms of four one-dimensional normal modes with wave numbers given by Eqs. (35) to (37). Equations (36) and (37) indicate that two modes may be interpreted as acoustic modes corresponding to right and left traveling acoustic waves. The remaining modes represent waves traveling with the flow. The wave defined by equation (35a) is unattenuated. However, this is not true for the wave defined by Eq. (35b) since in this paper κ_s/τ_s is assumed to be small. Thus, the attenuation of the wave traveling with the flow calculated by substituting Eq. (35b) into Eq. (42) is very large and this wave is highly damped for the cases considered herein. Consequently, this mode quickly decays in the combustion duct system. The wave with wave number given by Eq. (35a) is assumed to have negligible effect on the system. Thus, the pressure, particle velocity, and pressure spectral structure are assumed to be determined only by the acoustic modes.

The state variable differential equation (Eq. (25)) depends upon four dependent variables: pressure, particle velocity, entropy, and bulk gas temperature. In the next section the non-acoustic modes are removed from this state variable differential equation. This produces an acoustic state variable systems differential equation which has two independent variables: pressure and particle velocity. However, the new acoustic wave number solutions are identical to the previous ones. The acoustic state variable systems differential equation is further simplified by use of a velocity potential function to create a single one-dimensional differential equation. This is the equation used to model the system.

Acoustic State Variable Formulation

The set of differential equations which has only the acoustic mode is obtained by neglecting the convective term, $u_o \frac{\partial s}{\partial x}$ in Eq. (16). As a consequence Eq. (21) becomes

$$\frac{d}{d\theta}\left(\frac{s_1}{c_p}\right) = \frac{d}{d\theta}\left[\frac{(1-\gamma)}{\gamma}\frac{p_1}{p_o} + \frac{t_{1,\infty}}{t_{o,\infty}}\right] = -\frac{\kappa_s}{\tau_s}\frac{t_{1,\infty}}{t_{o,\infty}} \tag{43}$$

From this equation the response of the bulk gas temperature to a pressure perturbation is

$$\left(\frac{d}{d\theta} + \frac{\kappa_s}{\tau_s}\right)\frac{t_{1,\infty}}{t_{o,\infty}} = -\frac{d}{d\theta}\left(\frac{1-\gamma}{\gamma}\right)\frac{p_1}{p_o} \tag{44}$$

Taking the Fourier transform in the time domain of Eqs. (43) and (44) yields

$$\Phi\left[\frac{t_{1,\infty}}{t_{o,\infty}}\right] = -\frac{(-i\omega)(1-\gamma)}{[(-i\omega) + \kappa_s/\tau_s]}\Phi\left[\frac{p_1}{\gamma p_o}\right] \tag{45}$$

and

$$\Phi\left[\frac{s}{c_p}\right] = \frac{\mathcal{S}(\omega)}{c_p}\Phi\left[\frac{p_1}{\gamma p_o}\right] \tag{46}$$

where

$$\frac{\mathcal{S}(\omega)}{c_p} = \frac{(1-\gamma)}{1 + (-i\omega)\frac{\tau_s}{\kappa_s}} \tag{47}$$

The time Fourier transform of Eq. (15) is

$$\left[(-i\omega) + u_o\frac{\partial}{\partial x}\right]\Phi\left[\frac{u_1}{c_o}\right] + c_o\frac{\partial}{\partial x}\Phi\left[\frac{p_1}{\gamma p_o}\right] = 0 \tag{48}$$

Substituting Eq. (46) into the time Fourier transform of Eq. (24) yields

$$\left[(-i\omega) + u_o \frac{\partial}{\partial x}\right]\left[1 - \frac{\mathcal{S}(\omega)}{c_p}\right]\Phi\left[\frac{p_1}{\gamma p_o}\right] + c_o \frac{\partial}{\partial x}\Phi\left[\frac{u_1}{c_o}\right] = 0 \tag{49}$$

A plane wave solution to Eqs. (48) and (49) can be obtained in terms of a velocity potential, ψ, where

$$u_1 = -\frac{\partial \psi}{\partial x} \tag{50}$$

and

$$p_1 = \rho_o \left(\frac{\partial}{\partial \theta} + u_o \frac{\partial}{\partial x}\right)\psi \tag{51}$$

Substituting the time Fourier transform of Eqs. (50) and (51) into Eq. (49) yields a new governing partial differential equation called the non-adiabatic velocity potential wave equation

$$L\Phi[\psi] = \left[(-ik_s) + M_s \frac{d}{dx}\right]^2 \Phi[\psi] - \frac{d^2}{dx^2}\Phi[\psi] = 0 \tag{52}$$

where

$$c_s = \frac{c_o}{\left[1 - \frac{\mathcal{S}(\omega)}{c_p}\right]^{1/2}} \tag{53}$$

$$k_s = \omega / c_s \tag{54}$$

$$M_s = u_o / c_s \tag{55}$$

The velocity potential solution is assumed to be proportional to $\exp[(ik_o\mathcal{M})x - i\omega\theta]$. Substituting this solution into Eq. (52) yields a wave number equation which has the acoustic wave numbers given by Eqs. (36) and (37) as a solution. Consequently, the velocity potential wave equation solution consists of an acoustic wave traveling upstream and downstream expressed as

$$\psi = \left[a\, e^{(ik_o\Omega)^+ x} + b\, e^{(ik_o\Omega)^- x} \right] e^{-i\omega\theta} \tag{56}$$

In the following sections the use of the Fourier transform operator notation is discontinued since all variables such as ψ, p, and u are Fourier transformed variables.

APPLICATION TO DUCTED COMBUSTION SYSTEM

The analysis developed in the last section is now used to study the spectral structure of pressure measurements made in the ducted combustion system shown in Fig. 1. The ducted combustion system shown in Fig. 1 consists of: (1) a source region inside the combustor can; (2) a non-source region inside a spool piece and a long duct; (3) an area expansion and contraction on either side of a spool piece; and (4) an upstream boundary at the exit of the long duct and a downstream boundary at the combustor inlet.

The solution for the velocity potential in a non-source region is given by Eq. (56). The velocity potential wave equation (Eq. (52)) is assumed to apply in the source region with the addition of a source term $G(\omega,x)$ on the right hand side. Using the combustor inlet and exit impedance as a boundary condition a unique Green's function solution for the velocity potential is found. The acoustic pressure and particle velocity can be found from a velocity potential using Eqs. (50) and (51). Consequently, the acoustic pressure and particle velocity at the combustor exit can be determined from the velocity potential solution in the combustor. The acoustic pressure and particle velocity at the combustor exit can then be used to find the acoustic pressure and particle velocity at any other point in the ducted combustor system with four-pole equations in transfer matrix form derived using Equations (50), (51), and (56). The combustor exit impedance can be calculated

from the duct exit impedance using the same four-pole transfer matrix equations. The transfer matrix approach used is discussed in Refs. 14 to 17.

Source Region

The acoustic state vector approach developed in the last section is used to study the spectral structure of pressure measurements made in the ducted combustion system. The linear inhomogeneous velocity potential wave equation assumed to apply in the source region is

$$L\psi = G(\omega,x) \tag{57}$$

The boundary conditions at the combustor inlet and exit are respectively

$$\frac{Z_{CI}}{\rho_o c_o} = \frac{1}{\rho_o c_o}\frac{p_1}{u_1}\bigg|_{x=0} \tag{58}$$

and

$$\frac{Z_{CE}}{\rho_o c_o} = \frac{1}{\rho_o c_o}\frac{p_1}{u_1}\bigg|_{x=L_c} \tag{59}$$

In the following analysis, the combustion noise source is assumed to be acoustically compact in the x-direction. The volume source-distribution of monopole order confined to the duct cross-section $x = x_\ell$ is written as

$$G(\omega,x) = C_o \mathcal{H}(\omega)\delta(x - x_\ell)(1 - M_s^2) \tag{60}$$

Similar source descriptions have been previously applied by Mani (Ref. 18) to a fan noise problem and by Morfey (Ref. 19), Ingard and Singhal (Ref. 20), and Swinbanks (Ref. 21) to duct noise source problems.

Substituting Eqs. (52) and (60) into Eq. (57), and the time Fourier transform of Eqs. (50) and (51) into Eqs. (58) and (59) and some algebraic manipulation yields a problem that has the form of a general second order Sturm-Liouville differential equation with unmixed boundary conditions:

$$\mathcal{L}\psi = -\frac{d}{dx}\left(\varepsilon\frac{d\psi}{dx}\right) + \zeta\psi = \varepsilon C_o \mathcal{H}'(\omega)\delta(x - x_\ell) \tag{61}$$

$$\mathcal{B}_{CI}(0) = \left\{\left[\frac{Z_{CI}}{\rho_o c_o} + M_o\right]\frac{d\psi}{dx} + (-ik_o)\psi\right\}\Bigg|_{x=0} = 0 \tag{62}$$

$$\mathcal{B}_{CE}(L_c) = \left\{\left[\frac{Z_{CE}}{\rho_o c_o} + M_o\right]\frac{d\psi}{dx} + (-ik_o)\psi\right\}\Bigg|_{x=L_c} = 0 \tag{63}$$

where

$$\varepsilon = e^{-\left[\frac{2(-ik_s M_s)}{1 - M_s^2}\right]x} \tag{64}$$

and

$$\zeta = \frac{\varepsilon(-ik_s)^2}{1 - M_s^2} \tag{65}$$

However, since the differential equation has complex coefficients the operator $\mathcal{L}$ is not self-adjoint or Hermitian.

Since the differential equation is not self adjoint, the development of a solution in terms of an orthogonal set of eigenfunctions is more complex than obtaining a solution by constructing the Green's function solution (see Refs. 21 to 23). The Green's function solution is constructed using the two initial value solutions of the homogeneous equation

$$\mathcal{L}\psi = 0 \tag{66}$$

which satisfy Eqs. (62) and (63). This method is described in Refs. 24 and 25 where it is applied to self-adjoint operators. The solution to Eq. (66) with boundary condition given by Eq. (62) is

$$\psi_{CI} = a_{CI}\left[e^{(ik_o\Omega)^+x} + R_{CI}e^{(ik_o\Omega)^-x}\right] \tag{67}$$

where

$$R_{CI} = \frac{\left[\left(\frac{Z_{CI}}{\rho_o c_o} + M_o\right)\Omega^+ - 1\right]}{\left[1 - \Omega^-\left(M_o + \frac{Z_{CI}}{\rho_o c_o}\right)\right]} \tag{68}$$

The solution to Eq. (66) with boundary condition given by Eq. (63) is

$$\psi_{CE} = a_{CE}\left[e^{(ik_o\Omega)^+x} + R_{CE}e^{(ik_o\Omega)^-x}\right] \tag{69}$$

where

$$R_{CE} = \frac{\left[\left(\frac{Z_{CE}}{\rho_o c_o} + M_o\right)\Omega^+ - 1\right]}{\left[1 - \Omega^-\left(M_o + \frac{Z_{CE}}{\rho_o c_o}\right)\right]} e^{ik_o(\Omega^+ - \Omega^-)L_c} \tag{70}$$

Consequently, the Green's function solution to Eqs. (61) to (63) is given by

$$\mathcal{G}(\omega, x, x_\ell) = \begin{cases} -C_o\mathcal{H}(\omega)\dfrac{\psi_{CE}(x_\ell)\psi_{CI}(x)}{W(x_\ell)} & 0 < x < x_\ell < L_c \\ -C_o\mathcal{H}(\omega)\dfrac{\psi_{CI}(x_\ell)\psi_{CE}(x)}{W(x_\ell)} & 0 < x_\ell < x < L_c \end{cases} \tag{71}$$

where $W(x)$ is the Wronskian

$$W(x) = \psi_{CI}\frac{d}{dx}\psi_{CE} - \psi_{CE}\frac{d}{dx}\psi_{CI} \tag{72}$$

Using the time Fourier transforms of Eqs. (50) and (51), the pressure

and particle velocity Fourier transforms at the combustor exit are

$$p_1 = \rho_o \left[(-i\omega) + u_o \frac{\partial}{\partial x}\right] \mathcal{G}(\omega, x, x_\ell)\Big|_{x = L_c} \tag{73}$$

and

$$u_1 = -\frac{\partial}{\partial x} \mathcal{G}(\omega, x, x_\ell)\Big|_{x = L_c} \tag{74}$$

Equations (73) and (74) define the acoustic state vector at the combustor exit determined from the combustor inlet and exit boundary conditions and the source spectrum.

Duct Transfer Matrix

Substituting Eq. (56) into Eqs. (50) and (51) yields the pressure and particle velocity equations

$$p_1 = \rho_o c_o (-ik_o)\left[a_{11}ae^{(ik_o\Omega)^+ x} + a_{12}be^{(ik_o\Omega)^- x}\right] \tag{75}$$

and

$$u_1 = (ik_o)\left[a_{21}ae^{(ik_o\Omega)^+ x} + a_{22}be^{(ik_o\Omega)^- x}\right] \tag{76}$$

where

$$a_{11} = 1 - M_o\Omega^+ \tag{77}$$

$$a_{12} = 1 - M_o\Omega^- \tag{78}$$

$$a_{21} = \Omega^+ \tag{79}$$

and

$$a_{22} = \Omega^- \tag{80}$$

The integration constants a and b in Eqs. (75) and (76) are determined by assuming that $x = 0$, $p = p(0)$, and $u = u(0)$ at the left boundary and $x = L$, $p = p(L)$, and $u = u(L)$ at the right boundary. As a consequence, the relation between the acoustic state vector at $x = 0$, $\vec{Y}(0)$ and the acoustic state vector at L, $\vec{Y}(L)$ is

$$\vec{Y}(L) = \begin{pmatrix} p_1 \\ u_1 \end{pmatrix}_{x=L} = \begin{bmatrix} \alpha_{11} & \alpha_{12} \\ \alpha_{21} & \alpha_{22} \end{bmatrix} \begin{pmatrix} p_1 \\ u_1 \end{pmatrix}_{x=0} = [\alpha_{m,n}]\vec{Y}(0) \tag{81}$$

where

$$\alpha_{11} = \frac{a_{11}a_{22}e^{(ik_o\Omega)^+L_c} - a_{12}a_{21}e^{(ik_o\Omega)^-L_c}}{a_{11}a_{22} - a_{21}a_{12}} \tag{82}$$

$$\alpha_{12} = \rho_o c_o \frac{\left[-a_{11}a_{12}e^{(ik_o\Omega)^+L_c} + a_{11}a_{12}e^{(ik_o\Omega)^-L_c}\right]}{a_{11}a_{22} - a_{21}a_{12}} \tag{83}$$

$$\alpha_{21} = \frac{\left[a_{21}a_{22}e^{(ik_o\Omega)^+L_c} - a_{22}a_{21}e^{(ik_o\Omega)^-L_c}\right]}{\rho_o c_o (a_{11}a_{22} - a_{21}a_{12})} \tag{84}$$

and

$$\alpha_{22} = \frac{-a_{21}a_{12}e^{(ik_o\Omega)^+L_c} + a_{11}a_{22}e^{(ik_o\Omega)^-L_c}}{(a_{11}a_{22} - a_{21}a_{12})} \tag{85}$$

Discontinuity Transfer Matrix

The four-pole transfer matrix used at the junction of two pipes of different diameter is based on an acoustic energy conservation law. Various definitions for the acoustic energy in flowing fluid are given in Refs. 26-30. While none of these definitions are applicable to a plane wave propagating through a soot particle cloud in a flowing fluid, the method for finding an energy conservation equation used in Refs. 26 and 31 is applicable. The relationship which has the form of an acoustic energy conservation law is derived using Eqs. (48) and (49). A quantity corresponding to acoustic energy flux is defined by

$$N = \mathcal{J}_1 w_1 \tag{86}$$

where the acoustic energy per unit mass is

$$\mathcal{J}_1 = u_o u_1 + p_1/\rho_o \tag{87}$$

and the mass flux fluctuation rate is

$$w_1 = \rho_o u_1 + u_o \rho_1 \tag{88}$$

If Eq. (48) is multiplied by $w_1/\rho_o c_o$ and Eq. (49) by $\mathcal{J}_1/c_o^2$, the sum of the resulting second-order equations can be put in the form

$$(-i\omega)\frac{E}{c_o^2} + \frac{d}{dx}\left(\frac{N}{\rho_o c_o}\right) = 0 \tag{89}$$

where E represents an acoustic energy density

$$\frac{E}{c_o^2} = \left(\frac{u_1}{c_o}\right)^2 + \left[1 - \frac{\mathcal{S}(\omega)}{c_p}\right]2\left(\frac{u_o}{c_o}\right)\left(\frac{p_1}{\gamma p_o}\right)\left(\frac{u_1}{c_o}\right) + \left[1 - \frac{\mathcal{S}(\omega)}{c_p}\right]\left(\frac{p_1}{\gamma p_o}\right)^2 \tag{90}$$

and

$$\frac{N}{\rho_o c_o} = c_o\left[\frac{\mathcal{J}_1}{c_o^2}\right]\left[\frac{w_1}{\rho_o}\right] \tag{91}$$

Integrating Eq. (89) over a volume yields

$$\int_V (-i\omega) \frac{E}{c_o^2} (\omega) dV + \int_S \vec{N} \cdot \hat{n} d\sigma = 0 \tag{92}$$

since

$$\int_V \nabla \cdot \vec{F} dV = \int_S \vec{F} \cdot \hat{n} d\sigma \tag{93}$$

The area discontinuity is assumed to take place sharply at the junction of two pipes with different diameters causing the flowing gas to undergo a sudden expansion or contraction. As a consequence of Eq. (92), across the pipe discontinuity the acoustic energy is constant

$$N(1)S(1) = N(2)S(2) \tag{94}$$

To derive a transfer matrix across the discontinuity Eq. (94) is rewritten as

$$\mathcal{J}_1(1) = \mathcal{J}_1(2) \tag{95}$$

and

$$S(1)w_1(1) = S(2)w_1(2) \tag{96}$$

Algebraic manipulation shows that the acoustic state vectors on either side of the discontinuity are related by

$$\vec{Y}(x_1) = \left[B_{m,n}\right]\vec{Y}(x_2) \tag{97}$$

where the resulting transfer matrix is given by

$$\left[B_{m,n}\right] = \begin{bmatrix} 1 & \dfrac{\rho_o c_s M_s(2)\left\{\left[1 - \dfrac{S(2)}{S(1)}\right]^2\right\}}{1 - \left[\dfrac{S(2)}{S(1)} M_s(2)\right]^2} \\ 0 & \dfrac{S(2)\left[1 - M_s^2(2)\right]}{S(1)\left\{1 - \left[\dfrac{S(2)}{S(1)} M_s(2)\right]^2\right\}} \end{bmatrix} \tag{98}$$

System Boundary Conditions

First, the boundary condition at the duct exit is discussed. Experimental investigations of the exit impedance of flow ducts reported in Refs. 32 and 33 show the duct exit pressure reflection factor may be greater than unity. Theoretical investigations reported in Refs. 34, 35, and 36 show that the pressure reflection factor is greater than unity because of the flow field at the duct exit. The following empirical expression for $|R|$ is given in Ref. 20

$$R = 0.95\left[\frac{(1 - M_o)}{(1 + M_o)}\right]^{1.33} \qquad kr_d < 0.5 \tag{99}$$

where $|R|$ is measured at the upstream end of a duct. In the case of jet exit flow, M_o is replaced by $-M_o$ (Ref. 34). For case studied herein $|R|$ is about 1.03.

The model calculations shown herein are made using the following combustion duct exit pressure reflection factor

$$R = |R|e^{i\phi} = -\frac{(1 - M_o)}{(1 + M_o)}\left(\frac{1 - Z/\rho_o c_o}{1 + Z/\rho_o c_o}\right) \tag{100}$$

The duct exit impedance is

$$\frac{Z}{\rho_o c_o} = M_o + \left[1 - \frac{2J_1(\nu)}{\nu}\right] - \frac{i2S_1(\nu)}{\nu} \tag{101}$$

where

$$\nu = 2kr_d\Big/\sqrt{1 - M_o^2} \tag{102}$$

$J_1(\nu)$ is the Bessel function of the first order and first kind, $S_1(\nu)$ is the Struve function of the first kind and first order, and r_d is the duct radius. The duct exit impedance used was derived in Ref. 35 for a circular duct with flow having an open end fitted with an infinite acoustically rigid flange. Again, in the case of jet exit flow, M_o is replaced by $-M_o$ in Eqs. (100) to (101).

The other boundary condition is specified at the combustor entrance. To model the impedance the combustor entrance is taken to be closed by a rigid circular plate at the entrance. This corresponds to a zero particle velocity at $x = 0$. Consequently, the pressure reflection factor is unity at $x = 0$.

Calculation Procedure

The following procedure is used to calculate the pressure spectrum. It is applied at each frequency as necessary to obtain the desired spectrum. First, the exit pressure perturbation is arbitrarily assumed to be one Pascal. Then using the duct exit acoustic impedance based on the duct exit pressure reflection factor given by Eqs. (100) to (102), the particle velocity is calculated. Next, using the duct transfer matrix and the area discontinuity transfer matrix as necessary the acoustic state vector at the duct exit is used to find the acoustic state vector at the combustor exit. The resulting acoustic pressure and particle velocity are used to calculate the combustor exit impedance.

The next phase uses this impedance, the combustor entrance impedance, and a white noise source spectrum to determine the velocity potential solution in the source region. This velocity potential solution is used to calculate the acoustic pressure and particle velocity at the combustor exit due to the specified source and boundary conditions.

The last phase uses the duct transfer matrix and the area discontinuity matrix as necessary to calculate the acoustic state vector at any point in the duct from the acoustic state vector at the combustor exit. The pressure level at a given frequency is calculated from

$$(PL)_i = 10 \log_{10} \left[\widetilde{p_1^*(\omega,x_i) p_1(\omega,x_i)} \right] \qquad (103)$$

EXPERIMENTAL INVESTIGATION

The experimental apparatus is shown schematically in Fig. 1. The combustor section consists of a J-47 burner can placed concentrically in a 0.30 m diameter by 0.77 m long flow duct. The combustor section is followed by a 0.38 m diameter by 0.76 m long spool piece. This section is followed by a 0.30 m diameter by 6.1 m long flow duct.

The measurements discussed herein were made at an exit temperature of 920 K and at air mass flow rates of 0.5, 1.13, and 1.68 kg/sec. The corresponding velocities at the exit of the long duct were 18.5, 41.6, and 61.3 m/sec and the corresponding fuel flow rates were 0.009, 0.018, and 0.027 kg/sec. The fuel used was Jet A.

Simultaneous internal fluctuating pressure measurements were made at the three locations shown in Fig. 1. The transducers used were conventional 5/8 cm diameter (nominal) pressure response condenser microphones. To avoid direct exposure to the severe environment within the flow duct, the microphones were mounted outside the duct and the fluctuating pressure in the duct was communicated to the transducers by "semi-infinite" acoustic waveguides. The internal probes have previously been used for engine measurements (Refs. 37 to 39) and measurements in a combustion component test facility (Ref. 40). Probe design, frequency response, and operating characteristics are described in Ref. 41.

Measured constant-bandwidth pressure spectra are shown in Fig. 2 for duct exit flow velocities of 18.5, 41.6, and 61.3 m/sec. The spectra measured near the exit of the long duct are shown in Fig. 2(a) and the spectra measured near the entrance of the long duct are shown in Fig. 2(b). The structure of the measured spectra shown in Fig. 2(a) and 2(b) is similar at a given location for each test condition. The location of resonance peaks and dips is nearly

the same for each operating condition. Moreover, the peaks tend to be sharper at the low frequencies and more broad at the higher frequencies.

No attempt was made in this investigation to determine soot particle size or mass concentration. Data in the literacure indicates that typical soot particle diameters range from 0.05 μm to 1 μm (Ref. 42). Smoke concentration ranges from 0.53 to 5.8 gm/m^3 in the primary combustion zone and from 0.00018 to 0.015 gm/m^3 at a combustor exhaust station were found in Ref. 43. Besides being a function of position in the combustor, smoke concentration was found to be a function of combustor model, fuel-air ratio and operating pressure in Ref. 43.

COMPARISON WITH EXPERIMENTAL DATA

The model is used to calculate the pressure level near the beginning and end of the long duct. The parameters used to calculate the mass fraction and soot particle relaxation time used are given in Table I. The value of the soot particle soot relaxation time is assumed to be 1.5×10^{-6} sec for all cases. The following three values of mass fraction are used: 1.5×10^{-2}, 1.5×10^{-3} and 1.5×10^{-4}. The results obtained for a flow velocity of 18.5 m/sec are shown in Figs. 3 and 4.

The calculated spectra shown in Figs. 3 and 4 have similar structure even though the location of the peaks and their sharpness or broadness changes with mass fraction. The changes with mass fraction appear graphically in the form of stretching or as compression of the basic structure. These changes in the structure were easily recognized but proved difficult to simply explain.

The corresponding attenuation and sound propagation speed are shown in Fig. 5. For a mass fraction of 1.5×10^{-4} the sound propagation speed exhibited in Fig. 5 increases from the isothermal sound propagation speed of 510 m/sec to the adiabatic sound propagation speed of 609.0 m/sec before the frequency

has increased to 80 Hertz. Also, the attenuation is small at all frequencies. Model spectra calculated with a mass fraction of 1.5×10^{-4} are shown with the measured spectra in Figs. 3(a) and 4(a). Sharp resonant peaks appear in the calculated spectrum. In addition, the peaks are displaced from the broad peaks present in the measured spectrum.

For a mass fraction of 1.5×10^{-3} the sound propagation speed exhibited in Fig. 5 slowly increased from 510 m/sec to 610 m/sec. Also, the attenuation above 100 Hertz is above 0.5 dB. The calculated and the measured spectra exhibited in Figs. 3(b) and 4(b) are in good agreement for this mass fraction. Both the measured and calculated spectra have an increase in the broadness of the spectral peaks with frequency. Also, the calculated locations of the peaks are close to the measured locations.

For a mass fraction of 1.5×10^{-2}, the sound propagation speed exhibited in Fig. 5 is isothermal and the attenuation is less than 0.5 dB/m. For this mass fraction the calculated spectra shown in Figs. 3(c) and 4(c) have the correct location of resonant peaks only at the low frequencies. Also, the peaks are all sharp. Discrepancies occur at the higher frequencies.

The agreement between the calculated and measured location of peaks in the spectrum obtained using a mass fraction of 1.5×10^{-3} is attributable to the variation with frequency of the calculated sound propagation velocity. At low frequencies the calculated sound propagation velocity is near the isothermal speed of sound. As previously noted, using the cross-spectra phase angle, the sound propagation velocity was found to be near the isothermal speed of sound (ref. 10). Thus, these results provide additional evidence that the sound propagation speed is near the isothermal speed of sound.

Calculations made using a mass fraction of 1.5×10^{-3} with three different flow velocities are shown in Fig. 6. The calculated pressure level at the exit

of the long duct changes slightly with the mean flow velocity at the low frequencies. While the change is greater at the higher frequencies it occurs predominantly in the spectrum level and not the frequency location of peaks. Consequently, these changes could not be observed in the measured spectra. However, the measured spectra shown in Fig. 2 for the three flow velocities have similar trends at the low frequencies. Accordingly, the spectra measured at the higher duct exit flow velocities is also in fair agreement with the model calculations made for a mass fraction of 1.5×10^{-3}.

Above 200 Hertz a broad peak occurs in the spectra measured at flow velocities of 41.6 and 61.3 m/sec. This resonance does not occur in the spectra measured at a flow velocity of 18.5 m/sec. Moreover, this resonance does not seem to be related to the duct modes observed at the lower frequencies. This resonance may be due to a feedback type of instability involving the combustion process and the duct acoustics. Consequently, the calculated spectrum is compared only with the spectrum obtained at a duct exit flow velocity of 18.5 m/sec.

DISCUSSION

Spectral Structure

The spectral structure for a given operating temperature and a given geometry is determined by the value of the ratio of the soot particle thermal relaxation time to the mass fraction. Using Eqs. (17) and (18) and the parameters in Table I, the soot particle concentration can be calculated from the soot particle radius for a given value of this ratio by

$$(nm_s) = \frac{4.84 \times 10^9 \left(r_s^2\right)}{(\tau_s/\kappa_s)}, \quad gm/m^3 \tag{104}$$

This function is plotted in Fig. 7 for the three values of this ratio considered herein. Also shown in Fig. 7 is the smoke number for a given soot

particle concentration as given in Ref. 43. The circled point in Fig. 7 at $r = 0.342$ μm and $(nm_s) = 0.567$ gm/m^3 corresponds to the value in Table I for $\tau_s/\kappa_s = 0.001$ sec which produced the spectral structure that most resembled the measured spectra. This particular point may be unrealistic since it corresponds to a large smoke number. However, any point on the $\tau_s/\kappa_s = 0.001$ sec line would also produce the same spectral structure. Consequently, these results, to this extent, are independent of the parameters used in Table I. Unfortunately, this also means that the method cannot independently be used to estimate the soot particle radius or mass concentration.

Figure 7 also indicates how the sound propagation velocity varies with soot particle radius and mass concentration at combustion noise frequencies. The sound propagation speed can be determined from Eqs. (36) to (40). The sound propagation speed is isothermal at frequencies for which $(\omega\tau_s/\kappa_s)$ is less than unity. Consequently, sound propagates isothermally at frequencies less than a corner of break frequency, f_b, given by

$$f_b = \frac{1}{2\pi(\tau_s/\kappa_s)} \tag{105}$$

Above the corner or break frequency the sound propagation speed is changing from isothermal to adiabatic. Along curves A, B, and C the break frequencies are respectively 15.91, 159.1, and 1591 Hertz. For $(\tau_s/\kappa_s) = 0.01$ (corresponding to curve A in Fig. 7) the speed of sound propagation exhibited in Fig. 5 is less than 540 m/sec at frequencies below 15.91 Hertz. Also, for $(\tau_s/\kappa_s) = 0.001$ (corresponding to curve B in Fig. 7) the speed of sound propagation exhibited in Fig. 5 is less than 540 m/sec at frequencies below 159.1 Hertz. Consequently, at combustion noise frequencies in the region above curve A in Fig. 7 the sound propagation speed is adiabatic. In the region below curve C the sound propagation speed is isothermal. However, along curve B a mixed propagation situation occurs at combustion noise frequencies.

The maximum amount of attenuation is difficult to determine from Eq. (42). However, it is possible to determine the frequency which maximizes the phase angle of $(ik_o\Omega)$. The attenuation at this frequency is about 54% of the maximum attenuation. Substituting Eq. (36) into Eq. (42) and maximizing the phase angle shows the phase angle maximum attenuation at any operating temperature, for M = 0.0, occurs at

$$f_{max} = \frac{\gamma 1/2}{(2\pi\tau_s/\kappa_s)} \tag{106}$$

The phase angle maximum attenuation is at this frequency

$$\alpha_{max} = 4.96 \frac{f_{max}}{c_o}, \text{ dB/m} \tag{107}$$

Thus, along curves A, B, and C in Fig. 7, the phase angle maximum attenuation occurs respectively at 18.83, 188.3, and 1883 Hertz and is respectively 0.15, 1.53, and 15.3 dB/m. The attenuation is respectively 0.2846, 2.846, and 28.46 dB/m at $f = 1.0x10^{99}$.

The measured spectra shown in Figs. 2(a) and 2(b) may have similar structure at each operating condition because the value of the ratio of the heat transfer time constant to mass fraction did not change much with operating condition and was approximately 0.001 sec.

On the other hand, if the broad peak above 200 Hertz, which occurs in the measured spectra taken at flow velocities of 41.6 and 61.3 m/sec, is due to feedback between the duct acoustics and the combustion process, then its occurrence at these operating conditions may be due to a decrease in acoustic damping of the longitudinal waves due to a change in soot mass fraction or radius at these operating conditions. This possibility suggests that soot particles can be used to control certain types of combustor instability.

Model Assumptions

In this study the soot particles are assumed to have a uniform temperature and no mass loss because these simple assumptions produced theoretical results which agreed with measurements and because they greatly simplified the analysis. The actual effect of a pressure perturbation on the temperature and mass equilibrium between a liquid or solid particle and a gas is a complex problem depending on at least the following influences:

1. Convective heat transfer to or from the particle.
2. Heat transfer within the particle.
3. Mass transfer to or from the particle.
4. Surface chemical reactions on a soot particle.
5. Liquid-vapor phase transitions of a droplet.
6. Radiative heat transfer. Radiative heat transfer is not an important factor in this case since the combustion duct operating temperatures are low.

Many models can be constructed which describe this problem for a soot particle. As an example, it is possible to analyze this problem by assuming instantaneous heat transfer within the particle and by using a pressure and temperature dependent surface chemical reaction which effects heat and mass transfer (Ref. 10). This model is complex and depends on many parameters.

In this paper the particles are assumed to have a uniform temperature. This is assumed to be due to some unspecified pressure and temperature dependent surface chemical reaction. The model produced is dependent on only the ratio of τ_s to κ_s.

It is possible to analyze this problem by ignoring surface chemical reaction effects on heat and mass transfer and by assuming instantaneous heat transfer within the particle. The resulting thermal relaxation time for a 1 μm particle is about 0.3 μsec which shows that this type of particle quickly

follows any temperature change and does not have a constant, uniform temperature. However, experiments show that smoke concentrations of soot particles are reduced as soot travels from a measuring station at the primary combustion zone to one at the combustor exhaust (Ref. 43). Consequently, surface chemical reactions cannot be ignored. Further study is needed to discover what assumptions are best for analyzing this problem.

CONCLUDING REMARKS

A model for acoustic plane wave propagation in a combustion duct through a confined, flowing gas containing soot particles was presented. The model takes into account only heat transfer between the gas and soot particles. As a result, the model depends on only a single parameter which can be written as the ratio of the soot particle thermal relaxation time to the soot particle mass fraction. The model yields expressions for the attenuation and dispersion of the plane wave which depend only on this single parameter.

The model was used to calculate pressure spectra in a combustion duct. The results were compared with measured spectra. For particular values of the single free parameter the calculated spectra resemble the measured spectra. Consequently, the model, to this extent, explains the experimental measurements and provides some insight into the number and type of particles.

REFERENCES

1. Epstein, P. S. and Carhart, R. R., J. Acoust. Soc. Am. 25, 553-565 (1953).

2. Chow, J. C. F., J. Acoust. Soc. Am. 36, 2395-2401 (1964).

3. Temkin, S. and Dobbins, R. A., J. Acoust. Soc. Am. 40, 317-324 (1966).

4. Dobbins, R. A. and Temkin, S., AIAA J., 5, 2182-2186 (1967).

5. Morfey, C. L., J. Sound Vib., 8, 156-170 (1968).

6. Cole III, J. E. and Dobbins, R. A., J. Atmos. Sci., 27, 426-434 (1970).

7. Marble, F. E. and Wooten, D. C., The Pys. Fluids, 13, 2657-2664 (1970).

8. Davidson, G. A., J. Atmos. Sci., 32, 2201-2205 (1975).

9. Marble, F. E. and Candel, S. M., AIAA J., 13, 634-639 (1975).

10. Miles, J. H. and Raftopoulos, D. D., "Dispersion of Sound in a Combustion Duct by Fuel Droplets and Soot Particles," NASA TM 79236, 1979.

11. Cole III, J. E. and Dobbins, R. A., J. Atmos. Sci., 28, 202-209 (1971).

12. Polis, M. P. and Goodson, R. E., Proc. IEEE, 64, 45-61 (1976).

13. Conte, S. D. and de Boor, C., Elementary Numerical Analysis (McGraw-Hill, New York, 1972), pp. 74-83.

14. Igarashi, J. and Toyama, M., "Fundamentals of Acoustical Silencers. I - Theory and Experiment of Acoustic Low-Pass Filters," Rep. No. 339 Aeronaut. Res. Inst., Univ. of Tokyo, Vol. 24, No. 10 (1958).

15. Miwa, T. and Igarashi, J., "Fundamental of Acoustical Silencers. II - Determination of Four Terminal Constants of Acoustical Elements," Rep. No. 344. Aeronaut. Res. Inst., Univ. of Tokyo, Vol. 25, No. 4 (1959).

16. Igarashi, J. and Arai, M., "Fundamentals of Acoustical Silencers. III - Attenuation Characteristics Studied by an Electric Simulator," Rep. No. 351. Aeronaut. Res. Inst., Univ. of Tokyo, Vol. 26, No. 2 (1960).

17. Parrott, T. L., "An Improved Method for Design of Expansion Chamber Mufflers with Application to an Operational Helicopter," NASA TN D-7309 (1973).

18. Mani, R., ASME Trans., J. Basic Eng., 92, 37-43 (1970).

19. Morfey, C. L., J. Sound Vib., 14, 37-55 (1971).

20. Ingard, U and Singhal, V. K., J. Acoust. Soc. Am. 58, 788-793 (1975).

21. Swinbanks, M. A., J. Sound Vib., 40, 51-76 (1975).

22. Morse, P. M. and Feshbach, H., Methods of Theoretical Physics (McGraw-Hill, New York, 1953), pp. 884-886.

23. Kraft, R. E. and Wells, W. R., Acoust. Soc. Am. 61, 913-922 (1977).

24. Ref. 22, pp. 523-530.

25. Friedman, B., Principles and Techniques of Applied Mathematics (Wiley, New York, 1956), pp. 164-167.

26. Morfey, C. L., J. Sound Vib., 14, 159-170 (1971).

27. Möhring, W., J. Sound Vib., 18, 101-109 (1971).

28. Candel, S. M., J. Sound Vib., 41, 207-232 (1975).

29. Eversman, W., J. Sound Vib., 62, 517-532 (1979).

30. Tester, B. J., J. Sound Vib., 28, 205-215 (1973).

31. Bergman, P. G., J. Acoust. Soc. Am. 17, 329-333 (1946).

32. Mechel, von F., Schilz, W., and Dietz, J., Acustica, 15, 199-206 (1965).

33. Cummings, A., J. Sound Vib., 57, 261-279 (1978).

34. Lumsdaine, E., J. Sound Vib., 52, 145-147 (1977).

35. Lumsdaine, E. and Ragab, S., J. Sound Vib., 53, 47-61 (1977).

36. Mungur, P. and Plumblee, Jr., H. E., "Influence of the Jet Exhaust Flow Field on the Acoustic Radiation Impedance of a Jet Pipe Opening," AIAA Paper No. 79-0676 (March 1979).

37. Reshotko, M., Karchmer, A., Penko, P. F., and McArdel, J. G., "Core Noise Measurements on a YF-102 Turbofan Engine," AIAA Paper No. 77-21 (January 1977).

38. Karchmer, A. M., Reshotko, M., and Montegani, F. J., "Measurement of Far Field Combustion Noise From a Turbofan Engine Using Coherence Functions," AIAA Paper No. 77-1277 (October 1977).

39. Karchmer, A. and Reshotko, M., "Core Noise Source Diagnostics on a Turbofan Engine Using Correlation and Coherence Techniques," NASA TM X-73535 (1976).

40. Reshotko, M. and Karchmer, A., "Combustor Fluctuating Pressure Measurements In Engine and In a Component Test Facility - A Preliminary Comparison," NASA TM-73845 (1977).

41. Karchmer, A. M., "Identification and Measurement of Combustion Noise From a Turbofan Engine Using Correlation and Coherence Techniques," Ph.D. Thesis, Case Western Reserve Univ., Cleveland, Ohio (1978).

42. Linden, L. H. and Heywood, J. B., Combust. Sci. Technol., 2, 401-411 (1971).

43. Norgren, C. T., "Determination of Primary-Zone Smoke Concentrations from Spectral Radiance Measurements in Gas Turbine Combustors," NASA TN D-6410 (1971).

Table I. - Parameters used to calculate dispersion and attenuation due to soot particle-gas heat transfer

T, K	922.0
κ, W/m-k	5.38×10^{-2}
ρ_o, kg/M^3	0.378
c_p, J/kg-K	1100.0
γ	1.4
ρ_s, kg/M^3	1880.0
r_s, m	0.342×10^{-6}
c_o, m/sec	609.0
m_s, kg	3.15×10^{-16}
τ_s, sec	1.5×10^{-6}

Example

	1 Isothermal	2 Mixed	3 Adiabatic
n, number/m^3	1.8×10^{13}	1.8×10^{12}	1.8×10^{11}
nm_s, gm/m^3	5.67	0.567	0.0567
κ_s, Nm_s/ρ_o	1.5×10^{-2}	1.5×10^{-3}	1.5×10^{-4}
τ_s/κ_s, sec	1×10^{-4}	1×10^{-3}	1×10^{-2}

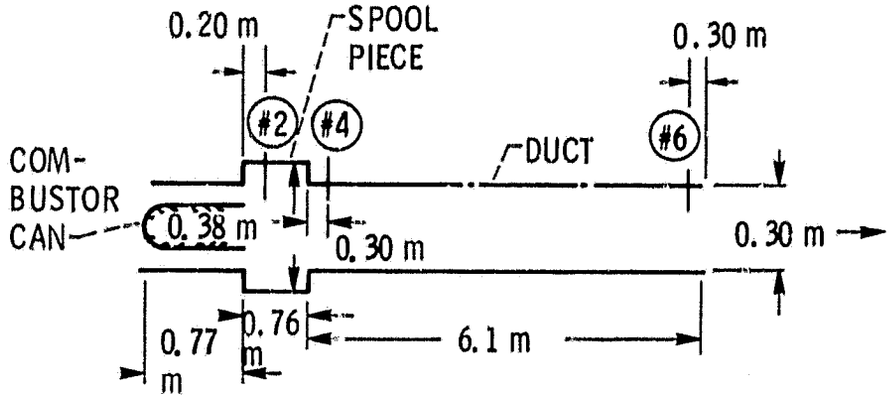

Figure 1. - Ducted combustion system.

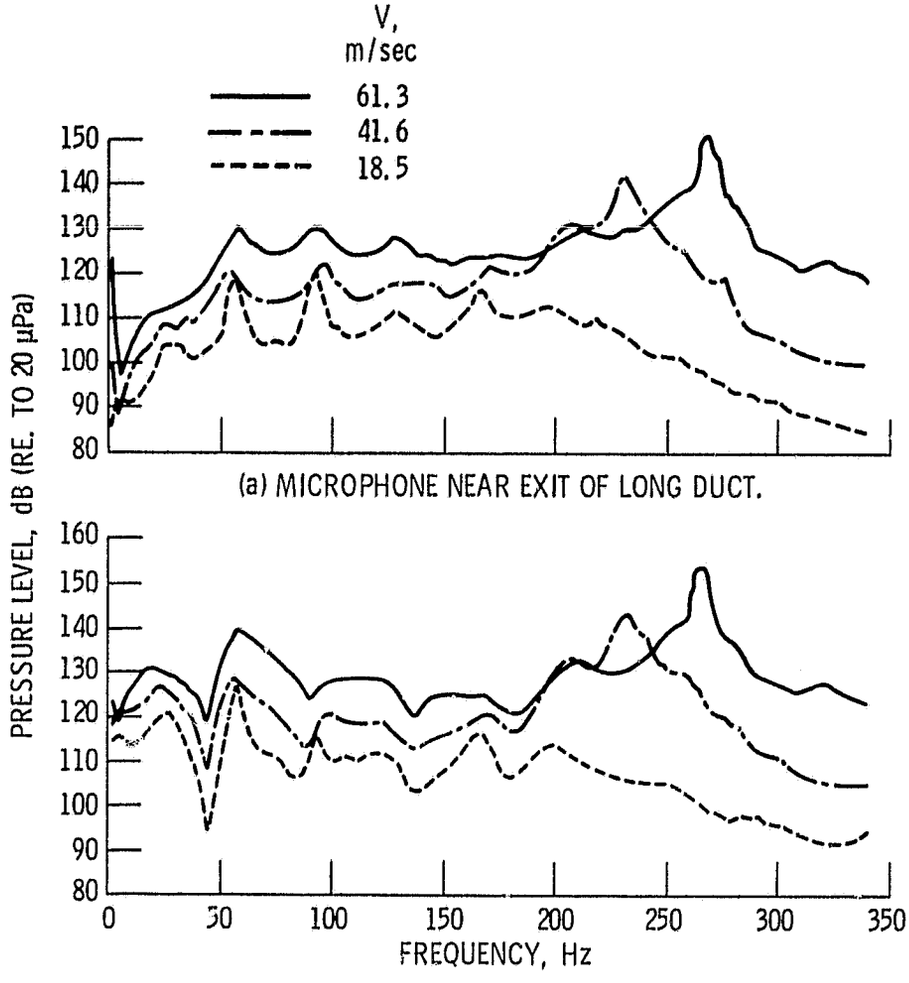

(a) MICROPHONE NEAR EXIT OF LONG DUCT.

(b) MICROPHONE NEAR ENTRANCE TO LONG DUCT.

Figure 2. - Measured pressure spectra.

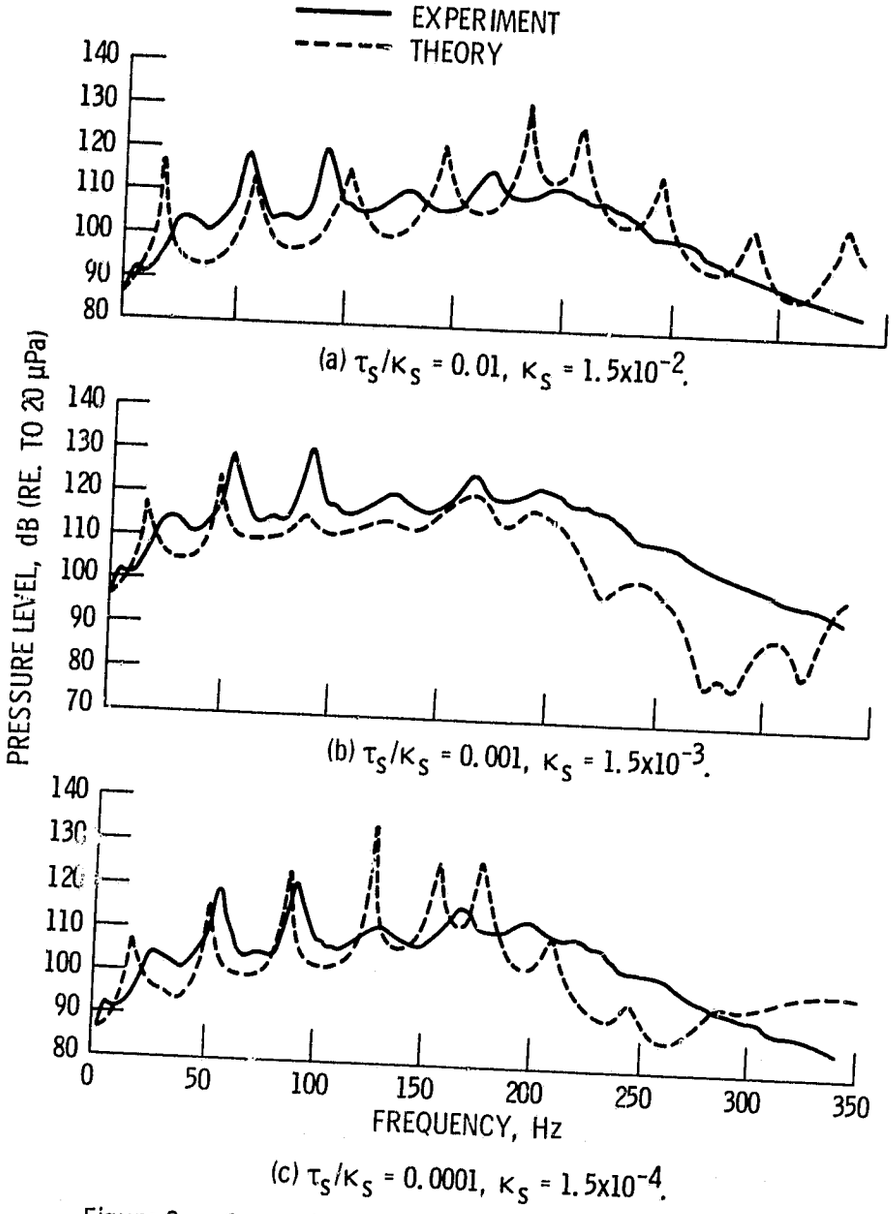

(a) $\tau_s/\kappa_s = 0.01$, $\kappa_s = 1.5 \times 10^{-2}$.

(b) $\tau_s/\kappa_s = 0.001$, $\kappa_s = 1.5 \times 10^{-3}$.

(c) $\tau_s/\kappa_s = 0.0001$, $\kappa_s = 1.5 \times 10^{-4}$.

Figure 3. - Comparison of measured and calculated pressure spectra near exit of long duct.

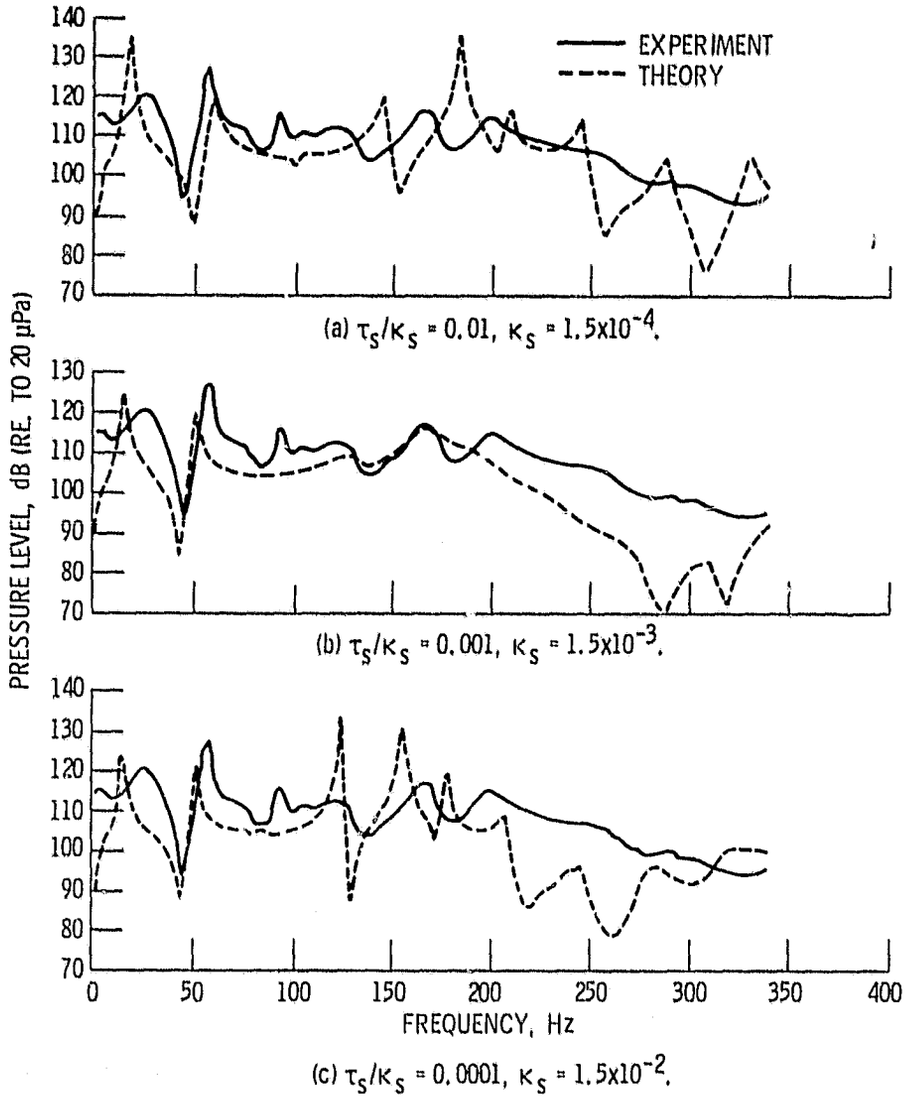

Figure 4. - Comparison of measured and calculated pressure spectra near entrance to long duct.

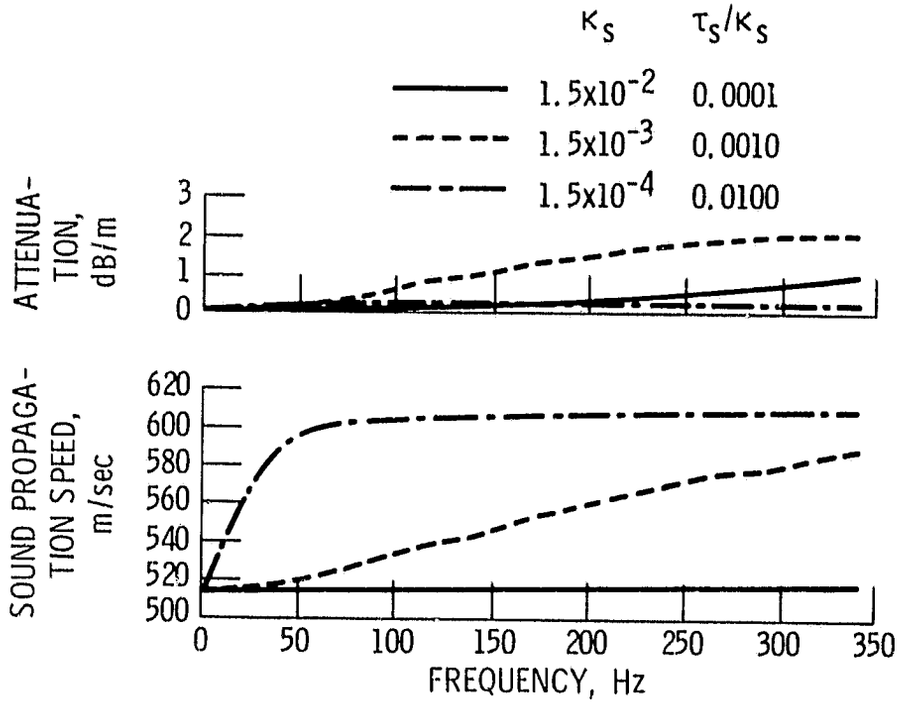

Figure 5. - Calculated attenuation and dispersion.

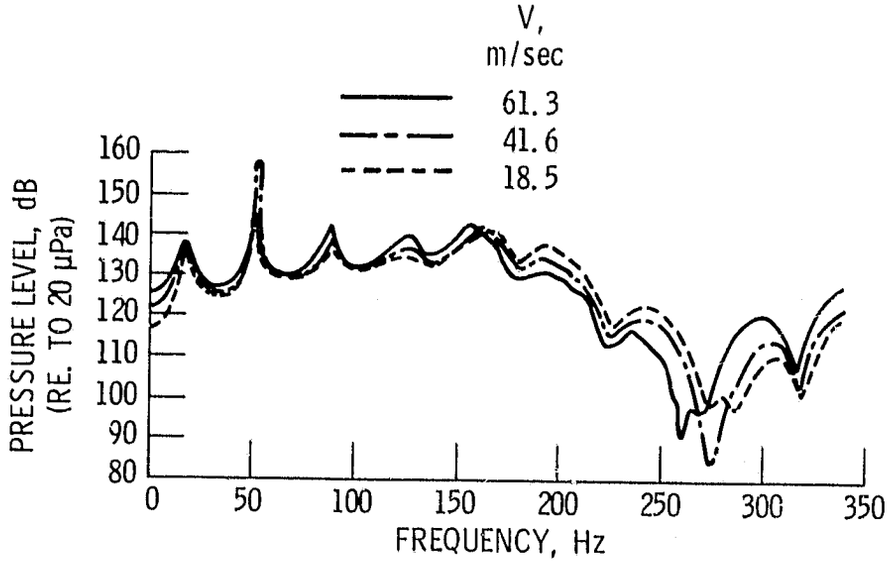

Figure 6. - Effect of flow velocity on computed pressure spectra: $\tau_s/\kappa_s = 0.001$, $\kappa_s = 1.5\times10^{-3}$.

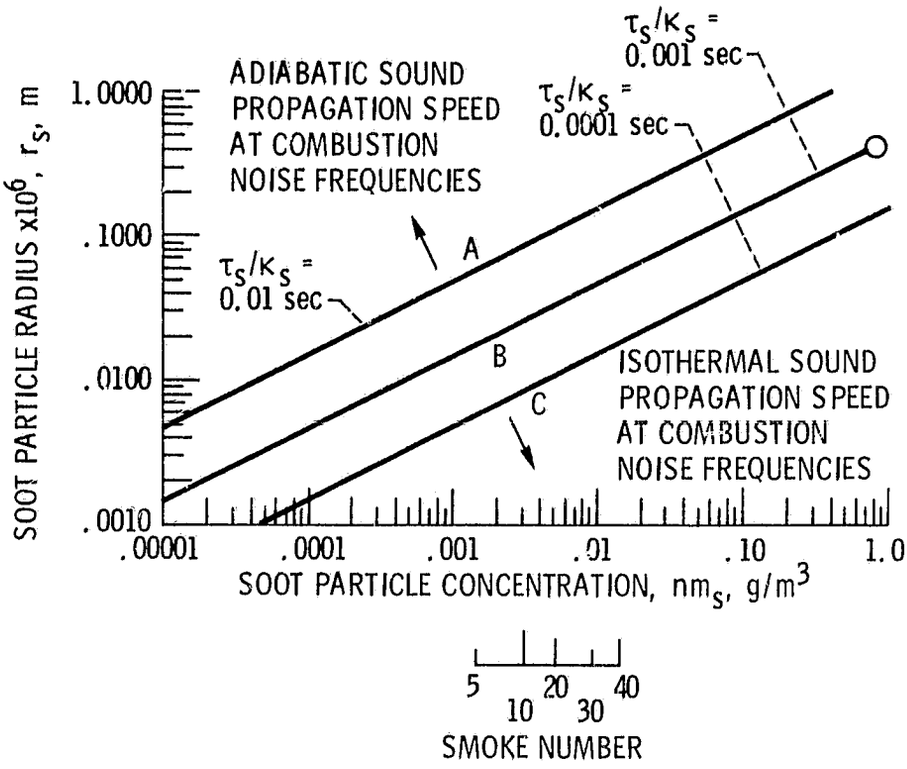

Figure 7. - Parameter map for τ_s/κ_s.